Journal of Materials Chemistry

PAPER

Significant enhancement of blue emission and electrical conductivity of N-doped graphene†

Tran Van Khai,[a] Han Gil Na,[a] Dong Sub Kwak,[a] Yong Jung Kwon,[a] Heon Ham,*[b] Kwang Bo Shim*[a] and Hyoun Woo Kim*[a]

Nitrogen (N)-doped graphene with different atomic percentages (2.3–4.7 at%) of N has been synthesized by thermal annealing of reduced graphene oxide (RGO) in ammonia gas for different times. The effects of annealing time on the structure, electrical and optical properties of N-doped graphene have been systematically investigated by using various analytical techniques. XPS, FTIR, Raman, and XRD studies show that there is a gradual structural change in N-doped graphene sheets with increasing annealing time, resulting from the increase of carbon and simultaneous decrease of oxygen and N contents. High resolution N1s spectra reveal that the pyridine-N and pyrrolic-N contents decrease with increasing annealing time, whereas the amount of quaternary-N increases. Importantly, it has been found that the annealing time caused significant changes in both the electrical and the optical properties of N-doped graphene. The electrical resistance of N-doped graphene is greatly reduced compared to that of GO and RGO, and found to further decrease with increasing annealing time, possibly due to the increase of sp^2 carbon networks and decrease of oxygen content as well as defects associated with the incorporation of N. The room-temperature photoluminescence (PL) properties of graphene oxide (GO), RGO and N-doped graphene were systematically studied with regard to the annealing time. The results showed that the PL spectrum of GO exhibits a peak emission maximum at around 700 nm, while that of RGO is found to be strongly blue-shifted with two distinct emission peaks: green emission at 485–500 nm and blue emission at 420–428 nm. For N-doped graphene samples, the blue emission intensity could significantly be enhanced by controlling the annealing time, which leads to a promising blue and green light-emitting material with controllable optical properties.

Introduction

Graphene, which is a single layer of sp^2-hybridized carbon atoms in a hexagonal two-dimensional lattice, has attracted tremendous attention due to its unique properties and potential applications.[1–6] In addition to the outstanding physical and chemical properties, graphene possesses novel optical properties,[7,8] which lead to the fabrication of important devices. Since material properties are usually related to the structure, many efforts have been made to modify the electrical properties and open the band gap of graphene by doping with other elements. In general, chemical doping with nitrogen (N) or boron (B) has been regarded as an effective method to intrinsically modify the

properties of carbon materials. Panchakarla *et al.*[9] reported that graphene doped with N and B demonstrated n- and p-type semiconducting electronic characteristics, respectively. Especially, N-doping plays a critical role in controlling the electronic and chemical properties of carbon materials due to its comparable atomic size and the availability of five valence electrons to form strong valence bonds with carbon atoms. It is revealed that N-doping results in the higher positive charge on carbon atoms adjacent to the N atoms,[10] and a positive shift of Fermi energy at the apex of the Brillouin zone of graphene.[11] The band gap of doped graphene can be adjusted by the level of doping.

Due to its special structure and extraordinary physical and chemical properties, N-doped graphene has been extensively applied in various fields, including electrochemical sensors,[12,13] biosensors,[14] electrocatalysis,[15,16] high-performance super-capacitors,[17] Li ion batteries,[18] solid state transistors,[19] light emitting diodes,[20] hydrogen storage[21] and fuel cells.[22,23] While many attempts have been made to explore the structural, electrocatalytic, and field emission properties of N-doped graphene, little work has been done on the investigation of electrical and optical properties.[24,25] The unique properties and potential

[a]*Division of Materials Science and Engineering, Hanyang University, Seoul 133-791, Republic of Korea. E-mail: hyounwoo@hanyang.ac.kr; kbshim@hanayng.ac.kr; Fax: +82-2-2220-0382*

[b]*H&H Co. LTD, Chungju National University, 50 Daehak-ro, Chungju-si, Chungbuk, 330-702, Korea*

† Electronic supplementary information (ESI) available: Experimental details, SEM images, raw scan XPS data, and a table of atomic concentrations. See DOI: 10.1039/c2jm33194b

applications of N-doped graphene can be explained by the way N atoms are incorporated into the sp^2-hybridized carbon network. It has been reported that the amount and type of N functionalities within N-doped graphene can be controlled by adjusting the synthetic conditions, such as the reaction temperature, the type of catalyst and the feedstock. In N-doped graphene sheets, four types of N atoms have been identified by X-ray photoelectron spectroscopy (XPS) studies: pyridine, pyrrolic, quaternary and oxidized pyridine-N. It is essential to understand the effect of the different N functionalities on the electrical conductivity and band gap of graphene, in order to tailor the N functionalities and thus to control the electrical and electronic properties of the graphene. To date, a variety of solution/solid techniques has been developed to synthesize N-doped graphene, including solvothermal methods,[26] hydrothermal reduction of colloidal dispersions of graphite oxide in the presence of hydrazine and ammonia,[27] thermal solid-state reaction of graphite oxide and urea,[28] and annealing of sandwich-layered substrates.[29] Furthermore, the vapor-phase methods, which can be easily and precisely controlled, have been intensively studied. These include the arc discharge method,[30] NH_3 annealing after N^+ ion irradiation of graphene,[31] NH_3 plasma exposure to graphene,[32] and adding NH_3 gas during chemical vapor deposition growth of graphene.[33]

In this paper, we report a simple and conventional approach to tune the content of N functionalities, electrical conductivity and optical properties of graphene, by means of thermal annealing of reduced graphene oxide (RGO) in an ammonia atmosphere at 1100 °C. The dependences of annealing time on the structural, electrical and optical properties of N-doped graphene were studied in detail.

Experimental

Materials

Graphite powder, H_2SO_4 (98%), H_3PO_4 (98%), $KMnO_4$ (98%), H_2O_2 (30 wt%), hydrazine monohydrate (98%), and N,N-dimethylformamide (DMF, 99.8%) were obtained from commercial resources and used as received.

GO was synthesized from graphite powder *via* a modification of Hummers and Offeman's method.[34] In a typical reaction, 5 g of graphite, 60 mL of H_3PO_4, and 180 mL of H_2SO_4 were stirred together with a Teflon-coated magnetic stirring bar in an ice bath. Next, 60 g of $KMnO_4$ was slowly added while the temperature was maintained at 0 °C. Once mixed, the solution is transferred to a 35 ± 5 °C water bath and stirred for 3 h, forming a thick paste. Next, distilled water (450 mL) was slowly dropped into the resulting paste to dilute the mixture, and then the solution was stirred for 1 h while the temperature was raised to 90 ± 5 °C. Finally, 800 mL of distilled water was added, followed by the slow addition of 60 mL H_2O_2 (30%), turning the color of the solution from dark brown to yellow. During this final step, H_2O_2 (30%) reduced the residual permanganate and manganese dioxide to colorless soluble manganese sulfate. The GO deposit was collected from the GO suspension by high-speed centrifugation at 15 000 rpm for 30 min. The obtained GO was then washed with 1000 mL of HCl (5%) and repeatedly washed with distilled water until pH = 7. To obtain uniform GO, a low-speed

centrifugation at 3000 rpm was first used to remove thick multilayer sheets until all the visible particles were removed (3–5 min). Then the supernatant was further centrifuged at 10 000 rpm for 30 min to remove small GO pieces and water-soluble byproducts. The final sediment was redispersed in 500 mL of DMF with mild sonication, resulting in a solution of exfoliated GO. In general, for chemically reduced GO (RGO), 500 mL of exfoliated GO was stirred for 30 min and 10 mL of hydrazine monohydrate was added. The mixtures were heated at 150 ± 5 °C in an oil bath for 24 h; a black solid precipitated from the reaction mixtures. Products were collected by centrifugation at 12 000 rpm for 45 min and washed with DI water and methanol until pH = 7. Next, the obtained RGO (as shown in Fig. S2†) was dried and stored in a vacuum oven at 60 °C until use.

Annealing RGO in NH_3

A horizontal alumina tube furnace was used for thermal annealing the RGO powders at 1100 °C under ammonia gas. In brief, the RGO powder (0.3 g) was put into the alumina boat, which was then introduced into the alumina tube reactor filled with Ar and HN_3 at atmospheric pressure. The system is first heated for 3 h at 250 °C to remove all the moisture with the mixture of NH_3 (20 sccm) + Ar (100 sccm). Subsequently the temperature is raised to 1100 °C for 90 min. The annealing reaction was carried out for 0.5, 1, 2, 3 and 4 h (corresponding to the samples: RGO at 0.5 h, RGO at 1 h, RGO at 2 h, RGO at 3 h and RGO at 4 h). Finally, the system was naturally cooled down to room temperature at a constant (Ar + NH_3) flow rate of 120 sccm.

The synthesized products were characterized by using a field-emission scanning electron microscope (FESEM, JSM-6700, JEOL Ltd., Tokyo, Japan) operated at an accelerating voltage of 12 kV. Transmission electron microscope (TEM) images were obtained on a JEOL JEM-2010 transmission electron microscope (JEOL Ltd., Tokyo, Japan) with an accelerating voltage of 200 kV. Atomic force microscope (AFM) images were obtained on an AFM XE-100 (Park system) equipment. X-ray diffraction (XRD) characterization was performed using a D/MAX Rint 2000 diffractometer model (Rigaku, Tokyo, Japan) with Cu Kα radiation (λ = 1.54178 Å, 40 kV, 200 mA). The Raman spectra were taken using a Jasco Laser Raman Spectrophotometer NRS-3000 Series, with an excitation laser wavelength of 532 nm, at a power density of 2.9 mW cm^{-2}. X-ray photoelectron spectroscopy (XPS, VG Multilab ESCA 2000 system, UK) analysis using a monochromatized Al Kα X-ray source ($h\nu$ = 1486.6 eV) was performed to analyze the elemental compositions and the assignments of the carbon peaks of the samples. The FTIR spectra (500–4000 cm^{-1}) were obtained using a Nicolet IR100 FTIR spectrometer. The current–voltage (I–V) characteristics of the samples were measured by the four probe method with an applied voltage ranging from −1.0 to 1.0 V using a source meter (Keithley Model 2400, OH, USA). PL spectra were acquired at room temperature using a SPEC-1403 photoluminescence spectrometer with the 325 nm line from a He–Cd laser (Kimon, Japan).

Results and discussion

An important factor determining the quality of graphene is the degree of oxidation and the presence of other hetero-atoms,

which affect the electrical and optical properties of the material. XPS is a powerful tool to identify the elemental composition in bulk materials. Furthermore, by analysis of binding energy (BE) values, we can detect the presence of oxygenated and nitrogenated groups. Fig. 1a–h show the XPS survey spectra of commercial graphite, GO, RGO and RGO annealed at 1100 °C in NH_3 gas for 0.5, 1, 2, 3 and 4 h, respectively. With carbon, oxygen and N species being detected, the atomic percentage (at%) of each element was calculated from the survey spectra (Fig. 1).

In the survey scan XPS spectra, the peaks at around 285.5, 399.8 and 534.0 eV correspond to the C1s, N1s and O1s corelevel, respectively. The chemical and thermal reductions seem to be effectively achieved, because the contents of oxygen atoms of RGO and thermally annealed RGO were significantly reduced, compared with that of GO. The oxygen content decreased in the
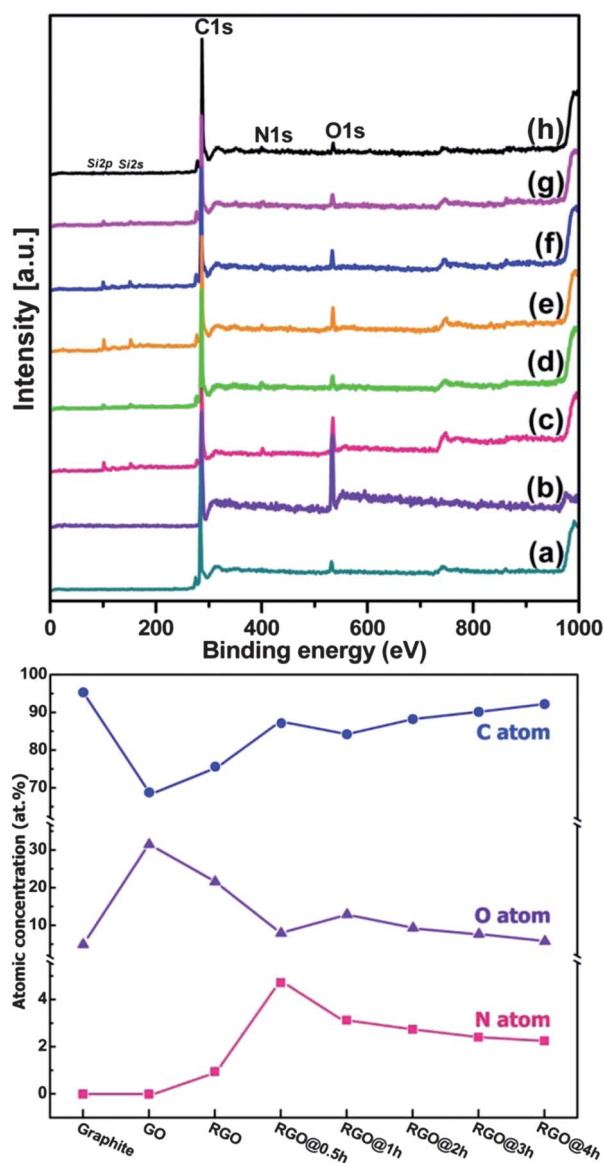
order of GO > RGO > annealed RGO, clearly indicating that thermal annealing is an effective method for removing the residual oxygen functional groups from the RGO. Therefore, thermal annealing after chemical reduction may further enhance the electrical properties of the RGO. In addition, it is found that the carbon content increased with increasing annealing time. Note that the N content decreased with increasing annealing time, possibly because the self-released oxygen from the RGO burnt N at high temperature. The highest doping level of 4.7 at% N is achieved at an annealing time of 0.5 h, which then gradually decreased to 2.3 at% N at an annealing time of 4 h. Hence, the chemical composition of N-doped RGO could be controlled by changing the annealing time. High resolution XPS of the asmade samples was performed to analyze the change of individual groups during the reduction processes. Note that the relative composition of individual groups was estimated by the percentage of the area of the relevant peak divided by the total area of all peaks (see ESI†). Fig. S2† shows the typical high resolution C1s XPS spectra of graphite and GO. The result clearly shows that the preparation of GO nanosheets from graphite using a modified Hummers' method introduces many oxygen-containing functional groups such as –COOH, –C=O, –C–O and –OH groups on the surfaces of the GO nanosheet. The content of oxygen element in the GO increased to 30.2 at% while the composition of C=C bonds decreased to 65.0%, which results from harsh oxidation and destruction of the sp^2 atomic structure of graphite.[35,36]

Fig. 2 shows high resolution C1s XPS spectra of as-synthesized RGO and RGO annealed for different times, exhibiting the relative composition of individual groups. After chemical reduction, the relative contribution of the components associated with oxygen in RGO was found to decrease significantly, in agreement with the previous literature.[37,38] It is worth noting that the content of oxygen element decreased to 21.31 at%, while the composition of C=C bonds increased to 74.0% in comparison to GO, clearly indicating a significant recovery of the sp^2 carbon network. In the case of unannealed RGO, the C1s peak can be fitted to six component peaks located at 284.6, 285.6, 286.2, 287.0, 288.0 and 288.9 eV. The peaks located at 284.6, 285.6, 287.0, 288.0 and 288.9 eV correspond to the energies of C=C, C–OH, C–O–C, C=O and COOH groups, respectively. Concurrently, a new component at around 286.2 eV can be ascribed to the C in the C=N bonds, resulting from bond formation during hydrazine reduction.[39,40] However, RGO still contained a large number of functional groups and defect sites. In the subsequent step, the residual functional groups were further removed by thermal annealing in NH_3. From the changes in the shapes of C1s XPS spectra before and after thermal annealing, it is clearly found that the residual oxygen functional group (C–OH) was reduced and some of them even disappeared (C=O and COOH groups), meanwhile the composition of C=C bonds increased up to 79.36% after annealing at 1100 °C for 0.5 h, indicating effective thermal reduction. With the further increase of annealing time, the residual oxygen functional groups continuously decrease with the simultaneous increase of the composition of C=C which approaches 82.70% (very close to the value of 87.95% of graphite) at an annealing time of 4 h. As shown in Fig. 2, the C1s XPS spectra of the annealed RGO samples can be fitted to five peaks located at around: 284.4–284.5, 285.4,

Fig. 1 Raw scan XPS spectra of (a) graphite powders, (b) GO, (c) RGO and RGO annealed for (d) 0.5 h, (e) 1 h, (f) 2 h, (g) 3 h and (h) 4 h; and their corresponding contents (bottom).
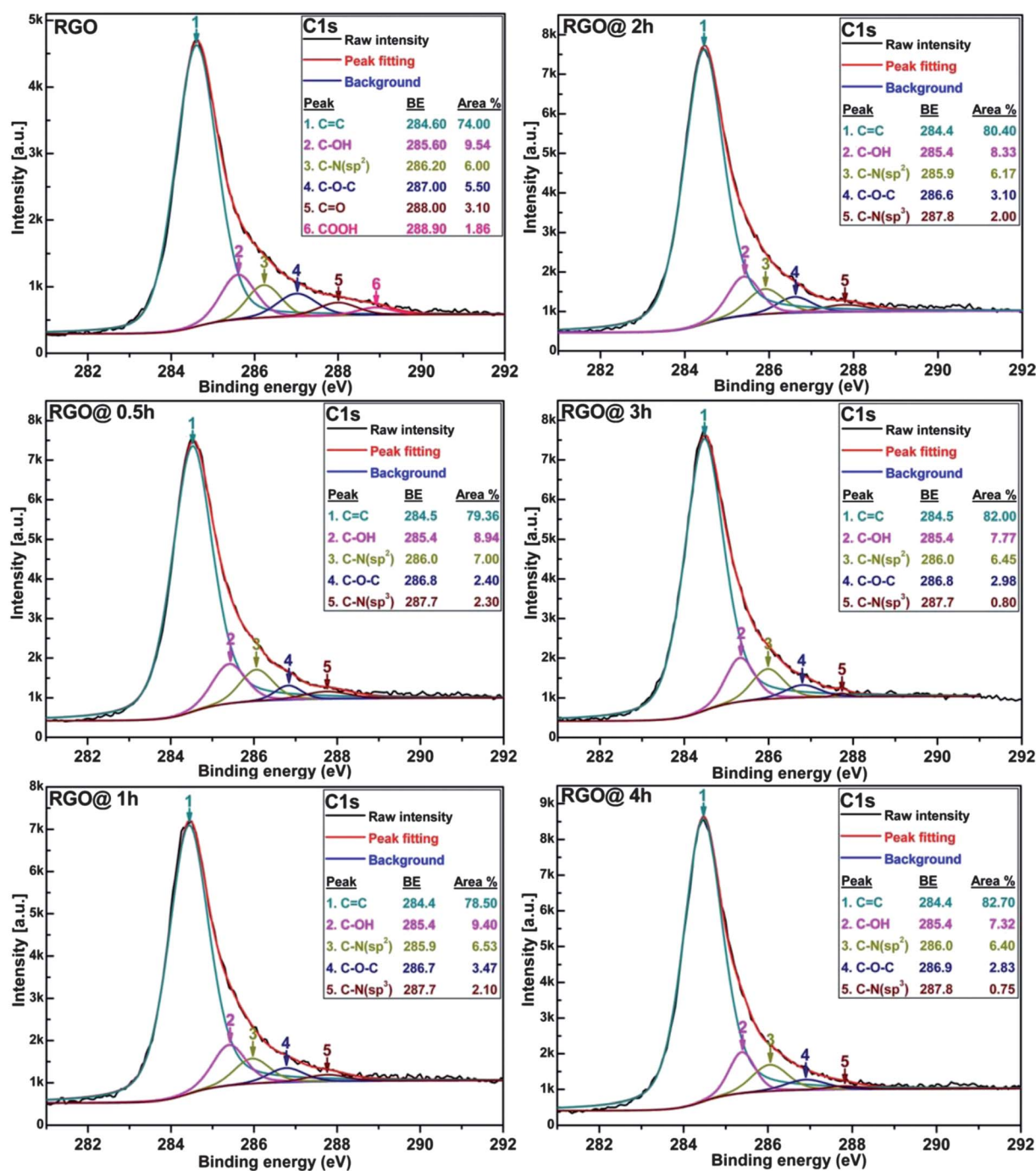
Fig. 2 High resolution C1s XPS spectra of RGO and RGO annealed for different times at 1100 °C.

285.9–286.0, 286.6–286.9 and 287.7–287.8 eV. The peaks located at 284.4–284.5, 285.4 and 286.8–286.9 eV can be attributed to the energies of C=C, C–OH and C–O–C, respectively. On the other hand, two peaks at 286.0 and 287.7 eV can be identified as two different C–N bonds, corresponding to N-sp^{2}C and N-sp^{3}C, respectively, originating from the substitution of the N atoms, defects or the edge of the graphene sheets.[41,42]

In addition, the formation of C–N bonds can also result from the reaction of the residual oxygen functional groups with NH$_3$,[19] which was confirmed by the further decrease of the O/C ratio in annealed-RGO (the O/C atomic ratio of RGO before and after

annealing at 1100 °C for 0.5 h is 0.31 and 0.87, respectively). Recent results demonstrated that the oxygen-containing functional groups in GO, such as carbonyl, carboxylic, lactone and quinine, were responsible for reactions with NH$_3$ to form C–N bonds and afford N-doping,[24] such as pyridine-N (*i.e.* the N atom is sp^2 hybridized bonding with two C atoms), pyrrolic-N (*i.e.* the N atom is sp^3 hybridized in a five-membered ring)[43] and/or quaternary-N (*i.e.* a C atom is substituted by a N atom in the graphitic sheet).[42] Hence, the number of oxygen-containing groups that remained in graphene sheets largely determined the final doping level of N. On the other hand, we found that

the annealing time was also an important factor that influences not only the chemical composition (as mentioned above) but also the type of N configuration in the graphene sheets. It is found that the total composition of N-sp^{2}C and N-sp^{3}C also decreased with increasing annealing time. The highest composition of N-sp^{2}C and N-sp^{3}C is achieved at an annealing time of 0.5 h, which then gradually decreases with the annealing time, which is consistent with the data shown in Fig. 1. Furthermore, it is observed that the ratio between the composition of N-sp^{2}C and N-sp^{3}C also changes with the annealing time, suggesting the possible contributions of different N structures in the different samples.

To further evaluate the chemical states of N before and after annealing, the high resolution N1s XPS spectra of as-synthesized RGO and RGO annealed for different times were measured and the results are shown in Fig. 3. For the as-synthesized RGO sample, the N1s spectrum can be fitted to two component peaks located at 398.2 and 399.9 eV, corresponding to pyridine-N and pyrrolic-N, respectively. The compositions of pyridine-N and pyrrolic-N are 71% and 29%, respectively, indicating that most of the N atoms incorporated into the RGO are in the form of pyridine-N. For RGO annealed at 1100 °C for 0.5 h, the high resolution N1s peak shows the presence of both pyridine-N and
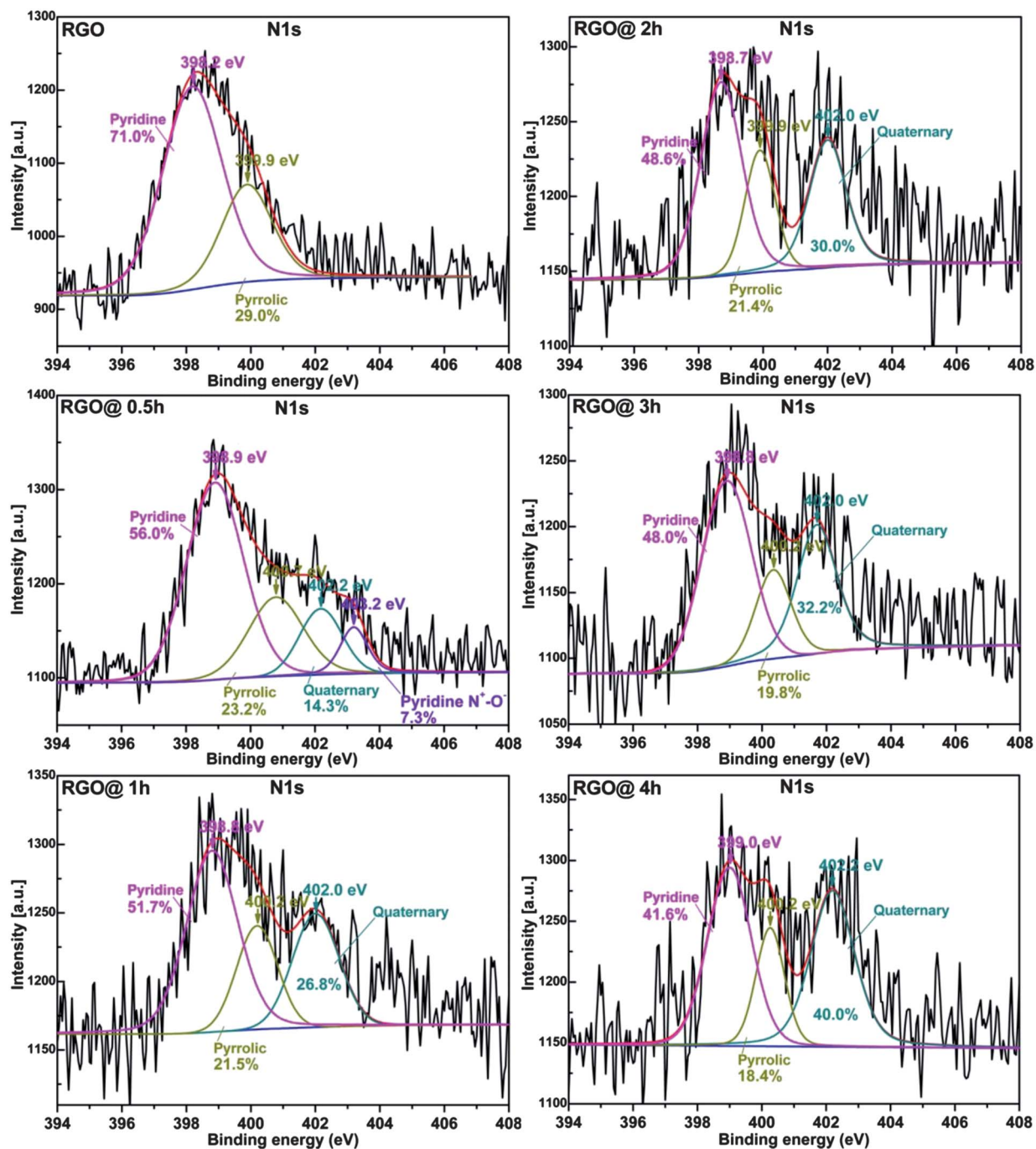
Fig. 3 High resolution N1s XPS spectra of RGO and RGO annealed for different times at 1100 °C.

pyrrolic-N atoms within the graphene sheets but is slightly shifted to higher energies of 398.9 and 400.7 eV, respectively. Additionally, it was found that compositions of both pyridine-N and pyrrolic-N decreased to 56.0 and 23.2%, respectively, suggesting that the pyridine-N and pyrrolic-N structures can be decomposed at elevated temperature. Besides the two peaks mentioned above, there are two new peaks that appear at 402.2 and 403.2 eV that can be attributed to quaternary-N and pyridine-$(N^+$–$O^-)$ in the graphene sheets, respectively.[44,45] In the pyridine-$(N^+$–$O^-)$ structure, the N atom is bonded to two carbon atoms and one oxygen atom. According to the literature, the pyridine-$(N^+$–$O^-)$ groups are formed when oxygen is present during the pyrolysis of N-containing carbon materials.[46,47] In this experiment, the reaction between oxygen and N during the annealing process is possible as the RGO contained a large amount of oxygen (~21.31 at%) and N (~1.58 at%).

With the further increase of annealing time, the composition of pyridine-N and pyrrolic-N gradually decreases, whereas the amount of quaternary-N increases, as shown in Fig. 3, suggesting that the pyridine-N and pyrrolic-N are weak structures and may become more unstable with increasing annealing time. The composition ratio of the quaternary-N to the total of pyridine-N and pyrrolic-N is estimated to be 0.18, 0.36, 0.40, 0.47 and 0.66 for annealing times 0.5, 1, 2, 3 and 4 h, respectively. The result indicates that longer annealing times would favor the formation of quaternary-N in the graphene sheets, while the shorter annealing times will lead to more incorporation of N in terms of pyridine-N and pyrrolic-N. Note that the pyridinic-$(N^+$–$O^-)$

peak disappears as the annealing time increases to 1 h. Hence, the N configuration in the graphene sheets could be controlled by adjusting the annealing time.

FTIR analysis of the as-made samples at different stages was conducted to provide the compositional and structural information of the samples. In this regard, Fig. 4a–g show the FTIR spectra of GO, RGO, RGO annealed for 0.5, 1, 2, 3 and 4 h, respectively. The curve of GO shows a stretching vibration of C=O at 1725 cm^{-1}, and two peaks at 3400 cm^{-1} and 1395 cm^{-1} corresponding to the stretching vibration and deformation vibration of OH.[48,49] The spectrum also shows two peaks at 1224 cm^{-1} and 1075 cm^{-1} originated from the C–O stretching vibrations of epoxy and alkoxy groups, respectively.[48,50] The peak at 1622 cm^{-1} is attributed to the O–H bending vibration of absorbed water molecules and the contributions from the vibration of aromatic C=C.[51] This result clearly shows that a large number of functional groups are introduced into carbon frameworks upon oxidation. However, after chemical reduction, the bands associated with oxygen-containing functional groups significantly decrease, and some of them even disappear, as shown in Fig. 4b. This shows that most functional groups of GO can be reduced by the chemical reaction with hydrazine monohydrate. Moreover, some new bands appear at 1556, 1406, and 1193 cm^{-1}, which correspond to the sp^2 C=N and/or aromatic C=C bonds,[52] sp^3 C–N mode[53,54] and C–C stretching, respectively. It is clear from the above observations that the sp^2 carbon networks of graphene sheets are restored and the N atoms are incorporated into the graphene lattice during chemical reduction.
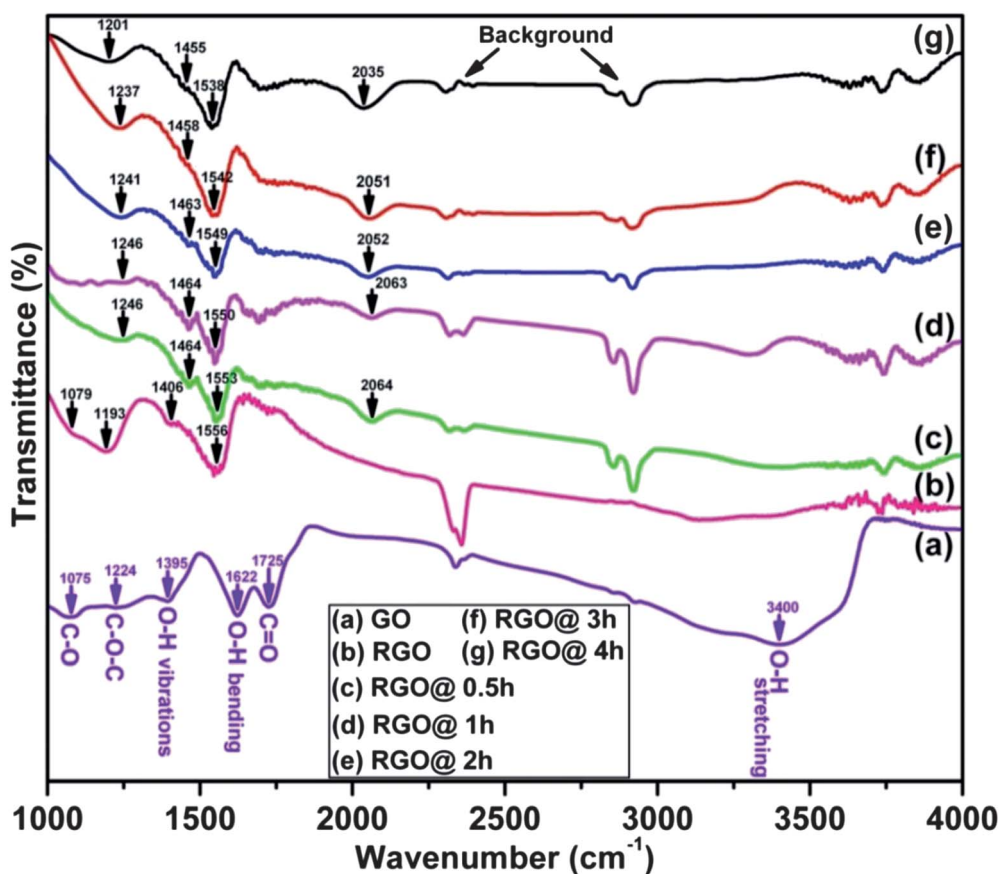
Fig. 4 FTIR spectra of (a) graphite powders, (b) GO, (c) RGO and RGO annealed for (d) 0.5 h, (e) 1 h, (f) 2 h, (g) 3 h and (h) 4 h at 1100 °C.

However, the stretching vibrations from C–O at 1079 cm^{-1} were still observed, which were caused by the remaining alkoxy groups even after hydrazine reduction. In the FTIR spectra of the annealed RGO samples, the band located at around 1538–1553 cm^{-1} can be assigned to the sp^2 C=N and/or C=C bonds. It is clearly seen that this band is shifted to lower frequency with the increase of the annealing time, suggesting an increased substitution of N at C sites in the graphene sheets. The band centered at around 1455–1464 cm^{-1} can be due to overlapping of the C–H bending vibration and C–N single bonds stretching vibration.[55] The intensities of these were found to rapidly decrease with the increase of the annealing time, suggesting that the C–N single bonds can be decomposed at a longer annealing time. The bands at around 1201–1246 cm^{-1} are attributed to originate from C–N stretching in the benzenoid rings.[56] Finally, the bands at around 2035–2064 cm^{-1} are related to triple bonds (C≡N) of nitriles.[57] Note that the position of all bands in the spectra of annealed RGO samples gradually shifted to lower frequency with increasing annealing temperature, revealing that the chemical modification of the RGO structure mainly occurred after the NH$_3$ treatment. The result of XPS combined with that of FTIR shows that carbon and N atoms are chemically bonded in the RGO sheets and mainly linked as triple C≡N, double C=N and/or single C–N bonds.

Raman spectroscopy is usually used to characterize the carbon materials. Fig. 5a–h (top) show Raman spectra of graphite, GO, RGO, and N-doped graphene annealed for 0.5 to 4 h at 1100 °C, respectively. Graphite has a prominent G band at 1582.3 cm^{-1} which is assigned to the first-order scattering of the E$_{2g}$ mode observed for sp^2 carbon domains and a broad D band at 1358.8 cm^{-1} is caused by sp^3-hybridized carbon, structural defects, carbon amorphous or edge planes that can break the symmetry and selection rule.[58] In the Raman spectrum of GO, the G band is broadened and shifted to 1597 cm^{-1}, while the D band at 1352 cm^{-1} becomes prominent, indicating the destruction of the conjugated system in graphite due to harsh oxidation by strong acids during the preparation. After GO was reduced to RGO, the D band became narrower and more prominent whilst the G band shifted from 1597 cm^{-1} to 1595.4 cm^{-1}, possibly due to the increase of the number of sp^2 carbons in the graphene sheets. Furthermore, as the RGO is annealed at 1100 °C, the position of the G band is further shifted to lower wavenumber in comparison with RGO, suggesting an efficient restoration of the sp^2 carbon networks in the graphene sheets through thermal annealing. In addition, it is observed that the G bands of N-doped graphene gradually shift to the position of the G band of graphite with the increase of the annealing time and decrease of the N concentration. It is interesting to note that the percentage of oxygen decreases with increasing annealing time, while the G-band shows a blue shift compared to that of GO and RGO. This suggests that a longer annealing time is more suitable for decomposition of oxygen containing functional groups and the restoration of sp^2 carbon networks. The intensity ratio of the D band to the G band (I_D/I_G) is usually used to measure the degree of graphitization of carbon materials. The calculated I_D/I_G ratios of graphite, GO, RGO and annealed RGO samples are shown in Fig. 5 (bottom). It is easily seen that the I_D/I_G ratio of GO is much higher than that of graphite, clearly indicating that GO has a higher distortion. After chemical reduction, the
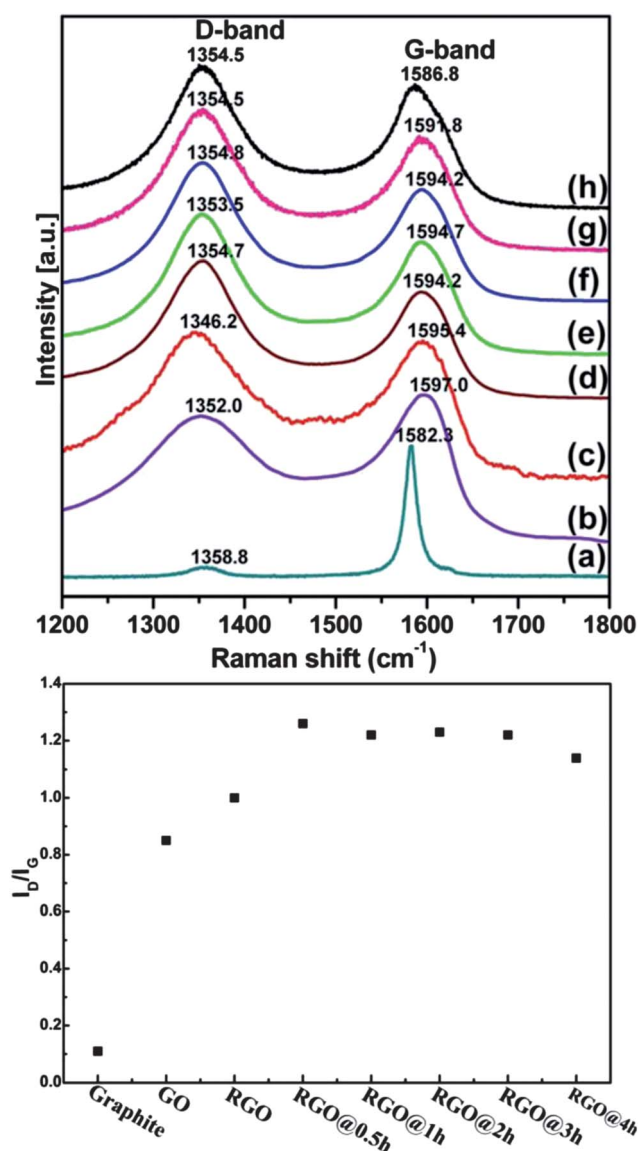
Fig. 5 Raman spectra of (a) graphite powders, (b) GO, (c) RGO and RGO annealed for (d) 0.5 h, (e) 1 h, (f) 2 h, (g) 3 h and (h) 4 h at 1100 °C; and their corresponding intensity ratios I_D/I_G (bottom).

I_D/I_G ratio of RGO continuously increased, indicating that more structural defects were added during chemical reduction.[59] Furthermore, after subsequent thermal annealing at 1100 °C for 0.5 h, the ratio of I_D/I_G was further increased, suggesting that thermal annealing further removed residual functional groups from the RGO, in good agreement with the XPS analysis. Also, a higher I_D/I_G ratio of N-doped graphene may result from the structural defects and edge plane exposure caused by the incorporation of heterogeneous N atoms into the graphene layers. Our result is in good agreement with those reported in the literature.[60,61] Nevertheless, with a further increase of the annealing time over 1 h, the ratio of I_D/I_G is found to decrease again, suggesting that the degree of long-range ordered crystalline perfection increases with increasing annealing time and decreases with N-doping (the N content decreases from 4.7 to 2.3 at% as the annealing time increases from 0.5 to 4 h). Hence, from the above results, it is concluded that the shift of G band position

and the increase in D band intensity could provide additional evidence for the incorporation of N atoms into carbon layers.[62]

We have further studied the effect of annealing time on the structural changes of graphene sheets using X-ray diffraction (XRD). As shown in Fig. 6a–h, raw graphite showed the very strong (002) peak at 26.40°, corresponding to an interlayer distance (d-spacing) of about 3.36 Å. However, after oxidation, the (002) peak shifted to a lower angle of around 11.11° and the d-spacing of GO increased to 7.95 Å. Such d-spacing is significantly larger than that of single-layer graphene (~3.40 Å), indicating that GO contains large numbers of oxygen-containing functional groups on both sides of the graphene sheets. In addition, the small bump near 18° indicates that the GO is not completely oxidized. However, after chemical reduction, a peak appears at 25.47°, corresponding to the d-spacing of 3.49 Å. It indicates that the bulk of oxygen-containing functional groups is removed from GO, resulting in the formation of much more distorted graphene sheets.[63,64] This is in agreement with the XPS, FTIR and Raman analyses. As the annealing time is increased, the peak at around 25.47° becomes more pronounced and sharper. The d-spacing is further reduced, approaching 3.37 Å at an annealing time of 4 h. The XRD results clearly show that thermal annealing enables a better ordering of the two-dimensional sheets. Note that the d-spacing of the N-doped RGO is slightly larger than that of graphite, being attributed to the presence of a small amount of residual oxygen-containing functional groups or other structural defects. In addition, a family of peaks observed for the N-doped RGO may be due to the formation of some crystalline carbon nitride phases. The peaks at

18°, 30.4° and 36.8° can be attributed to the graphitic carbon nitride (g-C_3N_4) phase.[65] The peaks at 31.5° and 51.8° can be ascribed to the α-C_3N_4 phase.[66–68] The other two peaks with diffraction angles (2θ) 33.8° and 49.2° are attributed to β-C_3N_4.[67,69] From Fig. 6, it seems that longer annealing times would favor the formation of more crystalline carbon nitride phases. All these carbon nitride phases (α-C_3N_4, β-C_3N_4) are predicted to be metastable with respect to the energetically most stable g-C_3N_4, they are believed to cause significant changes in the electrical and optical properties of the graphene sheets.

To study the effect of annealing time on the electrical conductivity of as-made samples, we investigated the current–voltage (I–V) characteristics using a four-point probe with a Keithley 2400 Source-meter. Fig. 7a–g show the I–V characteristics of GO, RGO and RGO annealed for different times, respectively. In order to examine the electrical conductivity, the GO/N-doped RGO films were prepared with the same thickness (see ESI†). It is found that all samples exhibit a linear I–V relationship with the voltage in the range of −1.0 to +1.0 V. The I–V slope of GO is close to zero and the smallest among the samples. This shows that GO behaves like a close-to-insulating material,[70] which can be attributed to the high oxygen content in the form of functional groups. It is widely known that the GO structure is predominantly amorphous due to distortions from the high fraction of sp³-O (C–OH, C–O–C, C=O and COOH). Moreover, due to the random distribution, the sp²-hybridized benzene rings are separated by sp³-hybridized rings, thus leading to the insulating characteristics.[71] However, the I–V slope of RGO significantly increased, indicating that the electrical conductivity
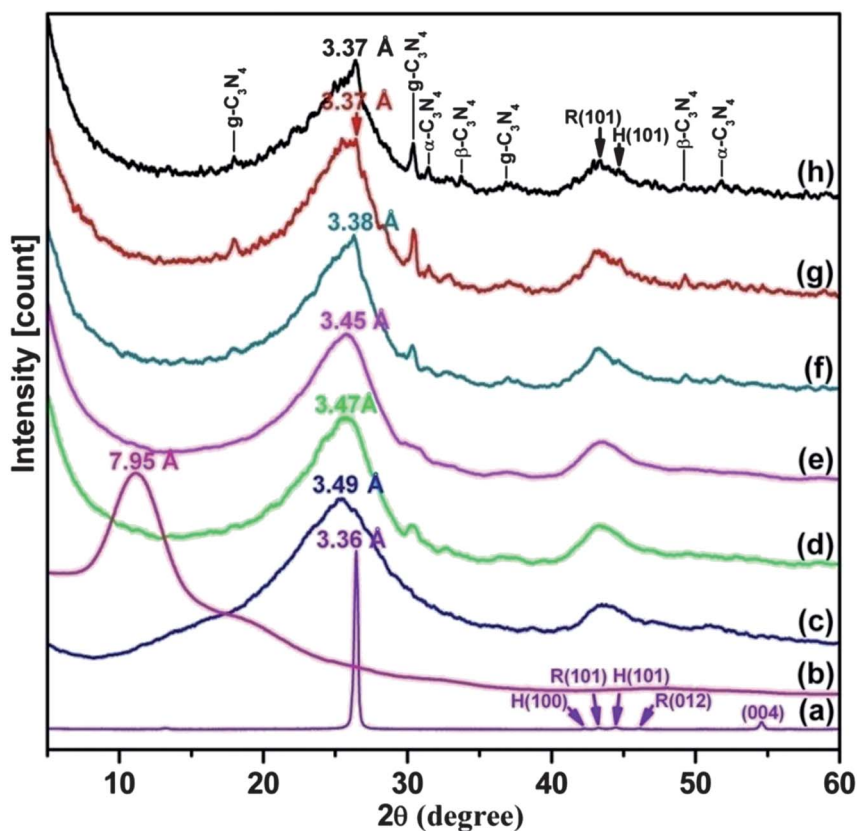
Fig. 6 XRD patterns of (a) graphite powders, (b) GO, (c) RGO and RGO annealed for (d) 0.5 h, (e) 1 h, (f) 2 h, (g) 3 h and (h) 4 h at 1100 °C.
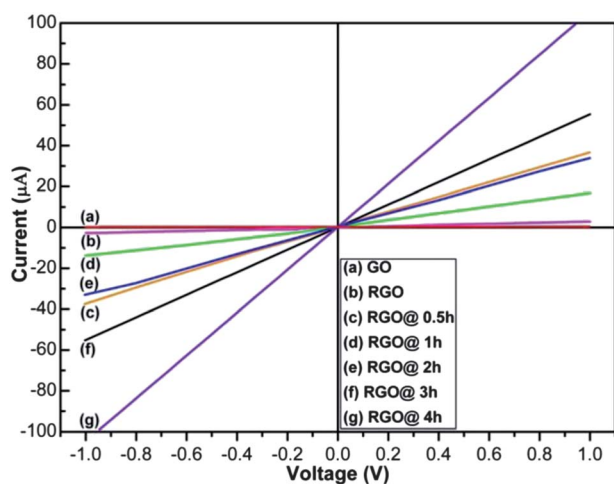
Fig. 7 Current–voltage curves of (a) GO, (b) RGO and RGO annealed for (c) 0.5 h, (d) 1 h, (e) 2 h, (f) 3 h and (g) 4 h at 1100 °C.

of RGO was considerably enhanced. The enhanced electrical conductivity of RGO can be due to the chemical removal of oxygen functional groups and simultaneous restoration of sp^2 carbon networks during chemical reduction. However, the electrical conductivity of RGO is still lower than that of graphite.[72] It implies that the structure of GO cannot be completely restored to graphitization by hydrazine monohydrate. To be suitable for practical applications, the conductivity of RGO needs to be improved. As a consequence of better ordering and additional deoxygenation by thermal annealing in NH_3, the electrical conductivity of RGO is found to increase further after 0.5 h annealing at 1100 °C. The graphitization temperature of carbon materials is known to be 1100 °C,[73] at which the residual oxygen functional groups in RGO will be completely eliminated,[74] contributing to the improvement of electrical conductivity. The improved electrical conductivity of GO on heating has been studied intensively.[24,75,76] On the other hand, we observed that the conductivity of RGO also depends on the annealing time. When the annealing time increases from 0.5 to 1 h, the conductivity of the RGO slightly decreases. This can be due to the higher oxygen content in the graphene sheets. However, as the annealing time further increases, the conductivity increases again and reaches the highest value for the sample annealed for 4 h. The I–V measurement data, in conjunction with XPS results, reveal that the conductivity of GO increases with increasing the content of sp^2 carbon networks and decreasing the oxygen content. Our result is in good agreement with that reported in the previous study.[24] However, it was also suggested that the electrical conductivity of carbon materials might be dependent on the amount of N atoms incorporated into their structure.[42,77,78] In the present study, the RGO sheets contain both O and N elements, giving them rich functionality (as shown by the XPS results). However, between O and N, it is very hard to distinguish which one is the main factor contributing to the electrical conductivity.

It was shown that thermal annealing of GO in NH_3-atmosphere is more effective than in other annealing atmospheres, such as Ar or H_2 gas.[24,76] With the appearance of quaternary-N at an annealing time of 0.5 h, the conductivity increased very rapidly,[60] and then gradually increased with increasing composition of quaternary-N as the annealing time is increased from 1

to 4 h. A more detailed study would be necessary in the future to further explore this. From the linear I–V curves, resistances of 6 MΩ, 300 kΩ, 27.27 kΩ, 60 kΩ, 29.29 kΩ, 16.20 kΩ and 8.30 kΩ were calculated for GO, RGO and RGO annealed for 0.5, 1, 2, 3 and 4 h, respectively. Accordingly, we suppose that the increase of electrical conductivity at longer annealing times is ascribed to better graphitization of sp^2 carbon networks of the graphene basal plane and to reduction of defects formed associated with the incorporation of N.[79,80] Hence, it can be concluded that the electrical conductivity of N-doped RGO is dependent on the annealing time.

Fig. 8 shows the room temperature PL spectrum of air-dried GO. Basically, the PL spectrum can be fitted to three peaks located at 600, 746 and 825 nm, which is similar to those obtained in previous studies.[81–83] It is well known that PL in amorphous carbon is due to the radiative recombination of electrons and holes (e–h) in the band-tail states created by rich sp^2 clusters.[84,85] These sp^2 clusters have opened heterogeneous electronic band gaps which are intrinsically correlated with their sizes, shapes, and fractions. In principle, large sp^2 clusters have narrower energy gaps than smaller ones; for example, a single benzene ring has an energy gap of around 7 eV, which decreases down to around 2 eV for a cluster of 30–40 aromatic rings.[86] Eda *et al.* speculated that emission in the ultraviolet-visible region can occur from sp^2 clusters with sizes of less than 1 nm amounting to ~20 aromatic rings. Larger sp^2 domains (>2 nm) possess smaller gaps, which may account for red to near-infrared emission. However, these calculations seem to provide only preliminary insight and are considered too simplistic because they do not take into account the influence of the surrounding sp^3 matrix as well as other sp^2 configurations (for example shape, symmetry and topology of the sp^2 chains and clusters) that might be present in GO. For our samples, the size of the sp^2 carbon clusters (designated as La) can be calculated from the intensity ratio between the D and G bands in the Raman spectra using Knight's empirical formula:[87]

$$La = 4.35/(I_D/I_G) \qquad (1)$$

The calculated size of sp^2 clusters is in the range of 5.10 to 3.45 nm and summarized in Table 1. It is found that the size of sp^2
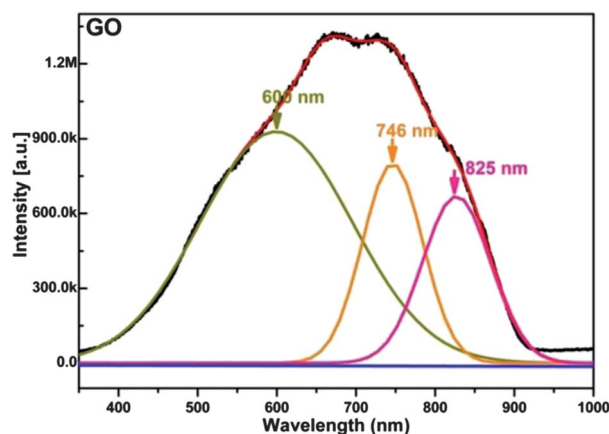
Fig. 8 Room temperature PL spectrum of GO.

Table 1 Size of sp² clusters of graphite, GO and RGO annealed for different times at 1100 °C. The crystalline size was calculated by employing the equation La = $4.35(I_D/I_G)^{-1}$

Sample	I_D/I_G	La (nm)
Graphite	0.11	39.5
GO	0.85	5.10
RGO	1.00	4.10
RGO at 0.5 h	1.26	3.45
RGO at 1 h	1.22	3.56
RGO at 2 h	1.23	3.56
RGO at 3 h	1.22	3.56
RGO at 4 h	1.14	3.80

cluster decreases in the order of GO > RGO > annealed-RGO. The size of sp² clusters of GO is ~5.10 nm. By using Raman, HRTEM and STEM-ADF analyses, one can also observe the sp² cluster of 2.5–8 nm in GO.[88–90] The larger sp² cluster of GO (~5.10 nm) led to the narrower band gap, which may account for orange-to-red emission. In contrast, the smaller sp² cluster (~3.80 to 4.10 nm) of RGO and annealed-RGO led to larger band gaps, which is responsible for the blue-green emission observed here.

In addition to those mentioned above, an alternative explanation for fluorescence in GO has been proposed by Pan *et al.*,[91] suggesting that the blue emission might have originated from free
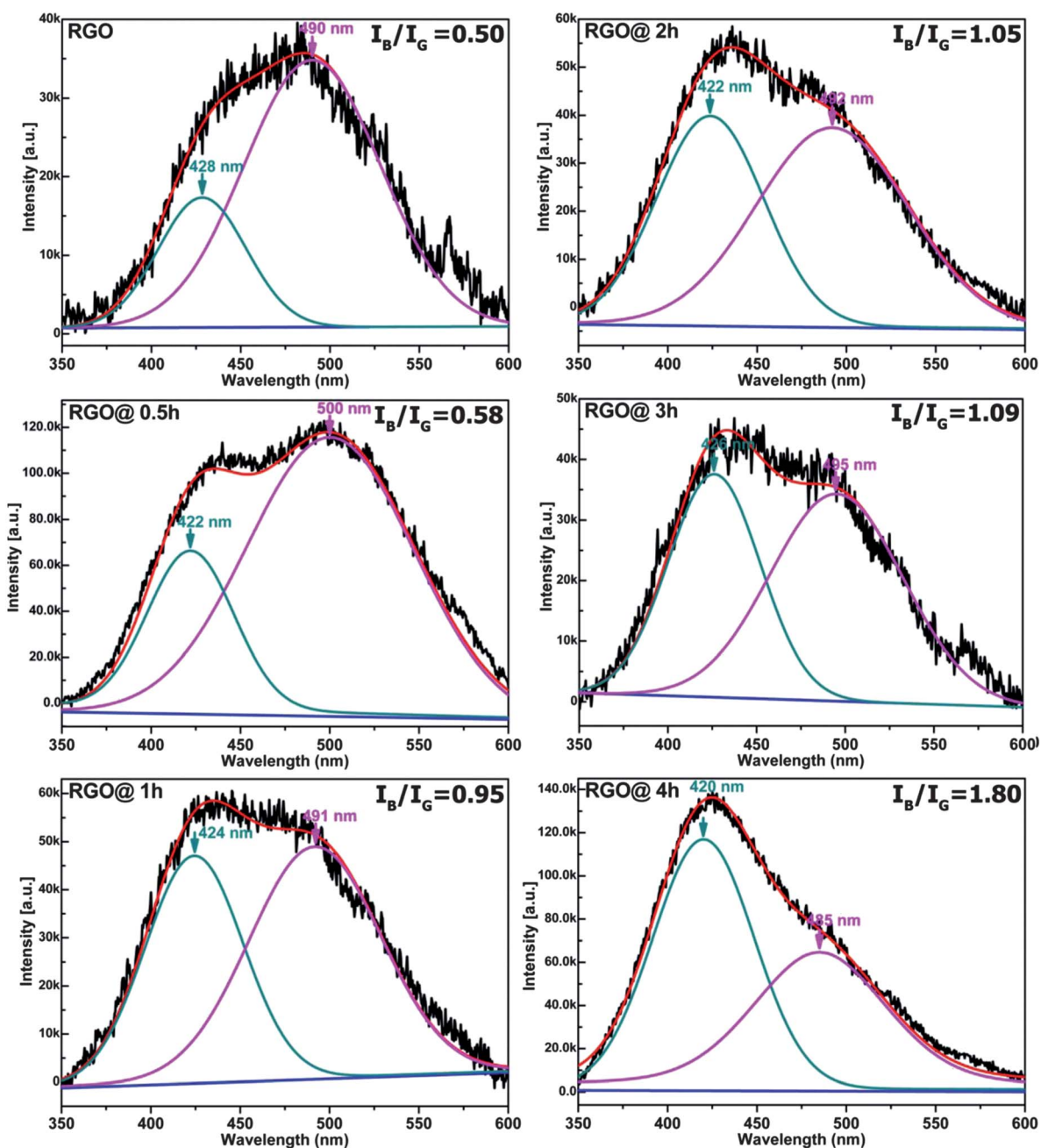
Fig. 9 Room temperature PL spectra of RGO and RGO annealed for different times at 1100 °C.

zigzag sites with a carbene-like triplet ground state described as $\sigma^1\pi^1$. Furthermore, fluorescence from carbon nanoparticles[92–94] and functionalized carbon nanotubes has been ascribed to the presence of oxygen-containing functional groups,[95] in a similar way to the mechanism reported for surface-oxidized silicon nanocrystals.[96] However, the observed enhancement of blue fluorescence with reduction suggests that oxygen functional groups can be excluded as the origin.[86,97,98]

Instead, the creation of localized sp^2 clusters and structural defects during the reductions are more likely to be responsible for the origin and enhancement of blue emission. Fig. 9 shows the PL spectra of RGO and annealed-RGO obtained at different annealing times. Being different from the case of GO, there are two bands in the RGO and N-doped samples: one is in the blue range of 420–428 nm, and the other is in the green range of 485–500 nm. All the bands are shifted to lower wavelengths than those obtained in GO, which can be due to the decreased sp^2 cluster size, defect level transition and structural changes. Interestingly, one can see that the intensity ratio between the blue and green bands significantly increases with an increase of the annealing time, with the position of these bands being slightly changed. It is well known that both the structure and defects affect the electronic structure of the nanomaterials, consequently changing their optical properties significantly.[99] Therefore, it is believed that pyridine-N and quaternary-N are two factors which contribute to the PL properties of RGO and annealed-RGO samples. After chemical reduction, it was found that the size of sp^2 clusters of GO decreased from 5.10 nm to 4.10 nm, indicating that chemical reduction easily caused nucleation of sp^2 domains in the sp^3 matrix and the density of small sp^2 nucleus increased, decreasing the average size of sp^2 domains and increasing the intensity ratio of I_D/I_G. In addition, the N atoms are incorporated into the graphene sheets in terms of pyridine-N and pyrrolic-N during chemical reduction. As a result of structural change, the PL spectrum of RGO shows the appearance of two peaks at 428 and 490 nm corresponding to the blue and green emission, while the peaks located at 600–900 nm disappear compared to that of GO. Thus, the creation of localized sp^2 clusters and structural defects during reduction[100] are likely to be responsible for the origin and enhancement of blue fluorescence. With increasing annealing time, the pyrrolic-N and pyridine-N contents decrease while the quaternary-N content increases, and as a result, the intensity ratio of blue to green bands (I_B/I_G) is greatly enhanced. It is likely that more incorporation of N in terms of quaternary-N into the graphene sheets can modify their electronic structure efficiently and allow them to enhance the blue emission. Our results are in good agreement with those reported in the previous study,[101] in which the PL intensity was significantly enhanced with the increase of the quaternary-N content.

Conclusions

In summary, N-doped graphene with different N contents (2.3–4.7 at%) was synthesized by thermal annealing RGO in NH_3. By using XPS, Raman, XRD, FTIR, PL and electrical measurements, it has been clearly shown that the annealing time strongly affected the structure, electrical and optical properties of N-doped graphene samples. The electrical resistance of N-doped graphene is much lower than that of GO and RGO, which is

attributed to the increase and decrease of carbon and oxygen contents, respectively, through thermal annealing. Additionally, it is shown that the further decrease in the electrical resistance of N-doped graphene at longer annealing times was ascribed to better graphitization of sp^2 carbon networks and decreased defects formed within the plane associated with the incorporation of N. On the other hand, it is noteworthy that carbon-based materials such as RGO or N-doped graphene give rise to blue emission. Moreover, the improvement of blue PL intensity of N-doped graphene can be achieved by increasing the annealing time. We suggest that PL in N-doped graphene is controlled by varying the pyridine-N, pyrrolic-N and quaternary-N contents.

Acknowledgements

References

1 O. C. Compton and S. B. T. Nguyen, *Small*, 2010, **6**, 711.
2 A. K. Geim and K. S. Novoselov, *Nat. Mater.*, 2007, **6**, 183.
3 C. Lee, X. Wei, J. W. Kysar and J. Hone, *Science*, 2008, **321**, 385.
4 A. A. Balandin, S. Ghosh, W. H. Bao, I. Calizo, D. Teweldebrhan, F. Miao and C. N. Lau, *Nano Lett.*, 2008, **8**, 902.
5 M. D. Stoller, S. Park, Y. Zhu, J. An and R. S. Ruoff, *Nano Lett.*, 2008, **8**, 3498.
6 Y. Zhang, Y. W. Tan, H. L. Stormer and P. Kim, *Nature*, 2005, **438**, 201.
7 S. A. Mikhailov and K. Ziegler, *J. Phys.: Condens. Matter*, 2008, **20**, 384204.
8 P. Avouvris, *Nano Lett.*, 2010, **10**, 4285.
9 L. S. Panchakarla, K. S. Subrahmanyam, S. K. Saha, A. Govindaraj, H. R. Krishnamurthy, U. V. Waghmare and C. N. R. Rao, *Adv. Mater.*, 2009, **21**, 4726.
10 K. Gong, F. Du, Z. Xia, M. Duratock and L. Dai, *Science*, 2009, **323**, 760.
11 S. U. Lee, R. V. Belosludov, H. Mizuseki and Y. Kawazoe, *Small*, 2009, **5**, 1769.
12 Y. Wang, Y. Shao, D. W. Matson, J. Li and Y. Lin, *ACS Nano*, 2010, **4**, 1790.
13 X. Huang, Z. Yin, S. Wu, X. Qi, Q. He, Q. Zhang, Q. Yan, F. Boey and H. Zhang, *Small*, 2011, **7**, 1876.
14 H. Fan, Y. Li, D. Wu, H. Ma, K. Mao, D. Fan, B. Du, H. Li and Q. Wei, *Anal. Chim. Acta*, 2012, **711**, 24.
15 Z. H. Sheng, L. Shao, J. J. Chen, W. J. Bao, F. B. Wang and X. H. Xia, *ACS Nano*, 2011, **5**, 4350.
16 Z. Luo, S. Lim, Z. Tian, J. Shang, L. Lai, B. MacDonald, C. Fu, Z. Shen, T. Yu and J. Lin, *J. Mater. Chem.*, 2011, **21**, 8038.
17 H. M. Jeong, J. W. Lee, W. H. Shin, Y. J. Choi, H. J. Shin, J. K. Kang and J. W. Choi, *Nano Lett.*, 2011, **11**, 2472.
18 A. L. M. Reddy, A. Srivastava, S. R. Gowda, H. Gullapalli, M. Dubey and P. M. Ajayan, *ACS Nano*, 2010, **4**, 6337.
19 Z. Jin, J. Yao, C. Kittrell and J. M. Tour, *ACS Nano*, 2011, **5**, 4112.
20 J. O. Hwang, J. S. Park, D. S. Choi, J. Y. Kim, S. H. Lee, K. E. Lee, Y.-H. Kim, M. H. Song, S. Yoo and S. O. Kim, *ACS Nano*, 2012, **6**, 159.
21 V. B. Parambhath, R. Nagar and S. Ramaprabhu, *Langmuir*, 2012, **28**, 7826.
22 L. T. Qu, Y. Liu, J. B. Baek and L. M. Dai, *ACS Nano*, 2010, **4**, 1321.
23 L.-S. Zhang, X.-Q. Liang, W.-G. Song and Z.-Y. Wu, *Phys. Chem. Chem. Phys.*, 2010, **12**, 12055.
24 X. Lin, H. Wang, J. T. Robinson, H. Sanchez, G. Diankov and H. Dai, *J. Am. Chem. Soc.*, 2009, **131**, 15939.
25 Z. Qian, J. Zhou, J. Chen, C. Wang, C. Chen and H. Feng, *J. Mater. Chem.*, 2011, **21**, 17635.
26 D. Deng, X. Pan, L. Yu, Y. Cui, Y. Jiang, J. Qi, W.-X. Li, Q. Fu, X. Ma, Q. Xue, G. Sun and X. Bao, *Chem. Mater.*, 2011, **23**, 1188.

27 D. Long, W. Li, L. Ling, J. Miyawaki, I. Mochida and S.-H. Yoon, *Langmuir*, 2010, **26**, 16096.
28 Z. Mou, X. Chen, Y. Du, X. Wang, P. Yang and S. Wang, *Appl. Surf. Sci.*, 2011, **258**, 1704.
29 C. Zhang, L. Fu, N. Liu, M. Liu, Y. Wang and Z. Liu, *Adv. Mater.*, 2011, **23**, 1020.
30 N. Li, Z. Wang, K. Zhao, Z. Shi, Z. Gu and S. Xu, *Carbon*, 2010, **48**, 255.
31 B. Guo, Q. Liu, E. Chen, H. Zhu, L. Fang and J. R. Gong, *Nano Lett.*, 2010, **10**, 4975.
32 Y.-C. Lin, C.-Y. Lin and P.-W. Chiu, *Appl. Phys. Lett.*, 2010, **96**, 133110.
33 D. Wei, Y. Liu, Y. Wang, H. Zhang, L. Huang and G. Yu, *Nano Lett.*, 2009, **9**, 1752.
34 W. S. Hummers and R. E. Offerman, *J. Am. Chem. Soc.*, 1958, **80**, 1339.
35 B. J. Jiang, C. G. Tian, L. Wang, Y. X. Xu, R. H. Wang, Y. J. Qiao, Y. G. Ma and H. G. Fu, *Chem. Commun.*, 2010, **46**, 4920.
36 M. Chouciar, P. Thordarson and J. A. Stride, *Nat. Nanotechnol.*, 2009, **4**, 30.
37 G. Eda, G. Fanchini and M. Chhowalla, *Nat. Nanotechnol.*, 2008, **3**, 270.
38 S. Park, J. An, R. D. Piner, I. Jung, D. Yang, A. Velamakanni, S. T. Nguyen and R. S. Ruoff, *Chem. Mater.*, 2008, **20**, 6592.
39 S. Standkovich, R. D. Pinter, X. Chen, N. Wu, S. B. T. Nguyen and R. S. Ruoff, *J. Mater. Chem.*, 2006, **16**, 155.
40 O. C. Compton, D. A. Dikin, K. W. Putz, L. C. Brinson and S. B. T. Nguyen, *Adv. Mater.*, 2010, **22**, 892.
41 D. C. Wei, Y. Q. Liu, Y. Yang, H. L. Zhang, L. P. Huang and G. Yu, *Nano Lett.*, 2009, **9**, 1752.
42 D. H. Lee, W. J. Lee and S. O. Kim, *Nano Lett.*, 2009, **9**, 1427.
43 S. van Dommele, A. Romero-Izquirdo, R. Brydson, K. P. de Jong and J. H. Bitter, *Carbon*, 2008, **46**, 138.
44 C. H. Choi, S. H. Park and S. I. Woo, *Green Chem.*, 2011, **13**, 406.
45 A. L. M. Reddy, A. Srivastava, S. R. Gowda, H. Gullapalli, M. Dubey and P. M. Ajayan, *ACS Nano*, 2010, **4**, 6337.
46 K. Stanczyk, R. Dziembai, Z. Piwowarska and S. Witkowski, *Carbon*, 1995, **33**, 1383.
47 J. R. Pels, F. Kapteijn, J. A. Moulijn, Q. Zhu and K. M. Thomas, *Carbon*, 1995, **33**, 1641.
48 C. Hontorialucas, A. J. Lopezpeinado, J. D. D. Lopezgonzalez, M. L. Rojascervantes and R. M. Martinaranda, *Carbon*, 1995, **33**, 1585.
49 Q. L. Shou, J. P. Cheng, L. Zhang, B. J. Nelson and X. B. Zhang, *J. Solid State Chem.*, 2012, **185**, 191.
50 V. Chandra and K. S. Kim, *Chem. Commun.*, 2011, **47**, 3942.
51 Y. X. Xu, H. Bai, G. W. Lu, C. Li and G. Q. Shi, *J. Am. Chem. Soc.*, 2008, **130**, 5856.
52 Z. J. Zhang, S. Fan, J. L. Huang and C. M. Lieber, *J. Electron. Mater.*, 1996, **25**, 57.
53 T. Szorenyi, C. Fuchs, E. Fogarassy, J. Hommet and F. L. Normand, *Surf. Coat. Technol.*, 2000, **125**, 308.
54 M. Ricci, M. Trinquecoste, F. Auguste, R. Canet, P. Delhaes, C. Guimon, G. Pfister-Guillouzo, B. Nysten and J. P. Issi, *J. Mater. Res.*, 1993, **8**, 480.
55 S. Kundoo, P. Saha and K. K. Chattopadhyay, *Adv. Appl. Ceram.*, 2006, **105**, 73.
56 M. R. Gizdavic-Nikolaidis, D. R. Stanisavljev, A. J. Easteal and Z. D. Zujovic, *J. Phys. Chem. C*, 2010, **114**, 18790.
57 L. M. Liao and C. X. Pan, *Soft Nanosci. Lett.*, 2011, **1**, 16.
58 A. C. Ferrari, J. C. Meyer, V. Scardaci, C. Casiraghi, M. Lazzeri, F. Mauri, S. Piscanec, D. Jiang, K. S. Novoselov and S. Roth, *Phys. Rev. Lett.*, 2006, **97**, 187401.
59 J. I. Paredes, S. Villar-Rodil, P. Solis-Ferander, A. Martinez-Alonso and J. M. D. Tascon, *Langmuir*, 2009, **25**, 5957.
60 Z. Mou, X. Chen, Y. Du, X. Wang, P. Yang and S. Wang, *Appl. Surf. Sci.*, 2011, **258**, 1704.
61 D. Geng, Y. Chen, Y. Chen, Y. Li, R. Li, X. Sun, S. Ye and S. Knights, *Energy Environ. Sci.*, 2011, **4**, 760.
62 R. Yadav, P. Dobal, T. Shripathi, R. Katiyar and O. Srivastava, *Nanoscale Res. Lett.*, 2009, **4**, 197.
63 M. J. McAllister, J. L. Li, D. H. Adamson, H. C. Schniepp, A. A. Abdala, J. Liu, M. Herrera-Alonso, D. L. Milius, R. Cao, R. K. Prud'home and I. A. Aksay, *Chem. Mater.*, 2007, **19**, 4396.
64 K. S. Subrahmanyam, S. R. C. Vivekchand, A. Govindaraj and C. N. R. Rao, *J. Mater. Chem.*, 2008, **18**, 1517.
65 K. Ramesh, M. Prashantha, N. Koteeswara Reddy and E. S. R. Gopal, *Integr. Ferroelectr.*, 2010, **117**, 40.
66 Y. P. Zhang, Y. S. Gu, X. R. Changa, Z. Z. Tiana, D. X. Shi, X. F. Zhang and L. Yuan, *Surf. Coat. Technol.*, 2000, **127**, 260.
67 D. W. Wu, W. Fan, H. X. Guo, M. B. He, X. Q. Meng and X. J. Fan, *Solid State Commun.*, 1997, **103**, 193.
68 S. Matsumoto, E. Q. Xie and F. Izumi, *Diamond Relat. Mater.*, 1999, **8**, 1175.
69 L. P. Ma, Y. S. Gu, Z. J. Duan, L. Yuan and S. J. Pang, *Thin Solid Films*, 1999, **349**, 10.
70 C. Gómez-Navarro, R. T. Weitz, A. M. Bittner, M. Scolari, A. Mews, M. Burghard and K. Kern, *Nano Lett.*, 2007, **11**, 3499.
71 P. G. Ren, D. X. Yan, X. Ji, T. Chen and Z. M. Li, *Nanotechnology*, 2011, **22**, 055705.
72 S. Stankovich, D. A. Dikin, R. D. Piner, K. A. Kohlhaas, A. Kleinhammes, Y. Jia, Y. Wu, S. B. T. Nguyen and R. S. Ruoff, *Carbon*, 2007, **45**, 1558.
73 H. A. Becerri, J. Mao, Z. F. Liu, R. M. Stoltenberg, Z. N. Bao and Y. S. Chen, *ACS Nano*, 2008, **2**, 463.
74 K. Kinoshita, in *Carbon: Electrochemical and Physicochemical Properties*, Wiley, New York, 1988.
75 M. Jin, T. H. Kim, S. C. Lim, D. L. Duong, H. J. Shin, Y. W. Jo, H. K. Jeong, J. Chang, S. Xie and Y. H. Lee, *Adv. Funct. Mater.*, 2011, **21**, 3496.
76 S. J. Wang, Y. Geng, Q. Zheng and J. K. Kim, *Carbon*, 2010, **48**, 1815.
77 F. Villapando-Peaz, A. Zamudio, A. L. Elias, H. Son, E. B. Barros, S. G. Chou, Y. A. Kim, H. Muramatsu, T. Hayashi, J. Kong, H. Terrosnes, G. Dresselhaus, M. Endo, M. Terrones and M. S. Dresselhaus, *Chem. Phys. Lett.*, 2006, **424**, 345.
78 J. D. Wiggins-Camacho and K. J. Stevenson, *J. Phys. Chem. C*, 2009, **113**, 19082.
79 I. K. Moon, J. Lee, R. S. Ruoff and H. Lee, *Nat. Commun.*, 2010, **73**, 1.
80 V. López, R. S. Sundaram, C. Cómez-Navarro, D. Olea, M. Burghard, J. Gómez-Herrero, F. Zamora and K. Kern, *Adv. Mater.*, 2009, **21**, 4683.
81 S. J. Henley, J. D. Carey and S. R. P. Silva, *Appl. Phys. Lett.*, 2004, **85**, 6236.
82 Z. Luo, P. M. Vora, E. L. Mele, A. T. C. Johnson and J. M. Kikkawa, *Appl. Phys. Lett.*, 2009, **94**, 111909.
83 T. V. Cuong, V. H. Pham, E. W. Shin, J. S. Chung, S. H. Hur, E. J. Kim, Q. T. Tran, H. H. Nguyen and P. A. Kohl, *Appl. Phys. Lett.*, 2011, **99**, 041905.
84 F. DeMichelis, S. Schreiter and A. Tagliaferro, *Phys. Rev. B: Condens. Matter*, 1995, **51**, 2143.
85 S. R. P. Silva, Rusli, J. Schwan, G. A. J. Amaratunga and J. Robertson, *Philos. Mag. B*, 1996, **74**, 369.
86 G. Eda, Y. Y. Lin, C. Mattevi, H. Yamaguchi, H. A. Chen, I. S. Chen, C. W. Chen and M. Chhowalla, *Adv. Mater.*, 2010, **22**, 505.
87 F. C. Tai, C. Wei, S. H. Chang and W. S. Chen, *J. Raman Spectrosc.*, 2010, **41**, 933.
88 K. Erickson, R. Erni, Z. Lee, N. Alem, W. Gannett and A. Zettl, *Adv. Mater.*, 2010, **22**, 4467.
89 G. Eda and M. Chhowalla, *Adv. Mater.*, 2010, **22**, 2392.
90 C. Mattevi, G. Eda, S. Agnoli, S. Miller, K. A. Mkhoyan and O. Celik, *Adv. Funct. Mater.*, 2009, **19**, 2577.
91 D. Pan, J. Zhang, Z. Li and M. Wu, *Adv. Mater.*, 2010, **22**, 734.
92 F. Wang, S. Pang, L. Wang, Q. Li, M. Kreiter and C. Y. Liu, *Chem. Mater.*, 2010, **22**, 4528.
93 H. Liu, T. Ye and C. Mao, *Angew. Chem., Int. Ed.*, 2007, **46**, 6473.
94 J. Zhou, C. Booker, R. Li, X. Zhou, T. K. Sham, X. Sun and Z. Ding, *J. Am. Chem. Soc.*, 2007, **129**, 744.
95 Y. Luo, X. Xia, Y. Liang, Y. Zhang, Q. Ren, J. Li, Z. Jia and Y. Tang, *J. Solid State Chem.*, 2007, **180**, 1928.
96 Y. Kanemitsu, S. Okamoto, M. Otobe and S. Oda, *Phys. Rev. B: Condens. Matter*, 1997, **55**, R7375.
97 K. S. Subrahmanyam, P. Kumar, A. Nag and C. N. R. Rao, *Solid State Commun.*, 2010, **150**, 1774.
98 J. L. Chen and X. P. Yan, *J. Mater. Chem.*, 2010, **20**, 4328.
99 X. G. Wan, J. M. Dong and D. Y. Xing, *Phys. Rev. B: Condens. Matter*, 1998, **58**, 6756.
100 G. Eda, C. Mattevi, H. Yamaguchi, H. Kim and M. Chhowalla, *J. Phys. Chem. C*, 2009, **113**, 15768.
101 J. Wen, Y. Zhang, N. Tang, X. Wan, Z. Xiong, W. Zhong, Z. Wang, X. Wu and Y. Du, *J. Phys. Chem. C*, 2011, **115**, 12329.